

# Nonlinear damping of the LC circuit using antiparallel diodes

Edward H. Hellen<sup>a)</sup> and Matthew J. Lanctot<sup>b)</sup>

*Department of Physics and Astronomy, University of North Carolina Greensboro, Greensboro, North Carolina 27402*

(Received 30 June 2006; accepted 26 January 2007)

We investigate a simple variation of the series RLC circuit in which antiparallel diodes replace the resistor. The result is a damped harmonic oscillator with a nonlinear damping term that is a maximum at zero current and decreases inversely with the current for currents far from zero. Unlike the standard RLC circuit, the behavior of this circuit is amplitude dependent. The transient response makes a transition from underdamped to overdamped behavior, and the resonance response of the steady-state driven oscillator becomes sharper as the source amplitude increases. A set of nonlinear differential equations is derived for the circuit and integrated numerically for comparison with measurements. The equipment is inexpensive and common to upper level physics labs. © 2007

*American Association of Physics Teachers.*

[DOI: 10.1119/1.2710481]

## I. INTRODUCTION

The series RLC circuit is a standard example of a damped harmonic oscillator. In this paper we investigate a simple variation of the RLC circuit in which the resistor is replaced by two antiparallel diodes as shown in Fig. 1. This circuit is fundamental in the sense that it is constructed from the most basic passive electrical components: inductor, capacitor, and diodes. Its behavior has interesting amplitude dependence not present in the standard RLC circuit due to the nonlinear current-voltage characteristics of the diodes. In particular, during the transient response there is a transition from underdamped to overdamped behavior. As a steady-state driven oscillator the resonance response becomes sharper as the source amplitude increases.

The use of antiparallel diodes creates a current-dependent damping term. We show in Sec. II that this circuit is described by the homogeneous nonlinear differential equation:

$$\frac{d^2i}{d\tau^2} + [b_0 + b_1(i)]\frac{di}{d\tau} + i = 0, \quad (1)$$

where

$$b_1(i) = \begin{cases} b/|i| & |i| \gg 1, \\ b & |i| \rightarrow 0. \end{cases} \quad (2)$$

Here  $i$  is the dimensionless current in the circuit,  $\tau$  is the dimensionless time,  $b_0$  is the familiar constant damping term, and  $b_1(i)$  is the current-dependent damping term. Thus damping is largest for  $i=0$  and decreases inversely and symmetrically about it. The nonlinearity of Eq. (1) is due to  $b_1(i)$ , which we show is responsible for the amplitude dependent behavior of the circuit.

The circuit's behavior can be inferred by inspection of Eqs. (1) and (2). For small current the damping term  $b_1(i)$  is large, creating an overdamped oscillator. For sufficiently large current the damping term decreases so that the circuit becomes an underdamped oscillator. Equation (1) is easily solved numerically using standard methods such as adaptive Runge-Kutta. We show that numerical computations agree with experimental measurements for both the transient response and the steady-state response to a sinusoidal source.

The circuit in Fig. 1 is similar to the extensively studied chaotic oscillator constructed from a sinusoidal signal gen-

erator driving the series combination of a resistor, inductor, and diode.<sup>1-5</sup> In these investigations interesting dynamics including chaos can occur when the reverse-recovery time of the diode is comparable to the circuit's natural oscillation period. For the diodes in Fig. 1 the reverse-recovery time (4 ns from the diode data sheet) is assumed to be zero because it is much shorter than the natural oscillation period,  $2\pi\sqrt{LC} \approx 30 \mu\text{s}$ . The nonlinear current-voltage relation of the diodes causes the interesting behavior in our case.

## II. CIRCUIT ANALYSIS

The sum of the voltage drops around the circuit in Fig. 1 and the time derivative gives

$$L\frac{d^2I}{dt^2} + R\frac{dI}{dt} + \frac{dV_d}{dt} + \frac{1}{C}I = \frac{dV_s}{dt}, \quad (3)$$

where  $V_d$  is the voltage across the antiparallel diodes. The resistor  $R$  accounts for the intrinsic resistance of the inductor in addition to any explicit resistors. For the transient response the right-hand side of Eq. (3) is zero.  $V_s$  is a sinusoidal source whose amplitude and frequency are varied.

The voltage  $V_d$  across the antiparallel diodes is a function of the current, so its time derivative is

$$\frac{dV_d}{dt} = \frac{dV_d}{dI} \frac{dI}{dt} = R_d(I) \frac{dI}{dt}, \quad (4)$$

where  $R_d(I) = dV_d/dI$  is the dynamic resistance of the antiparallel diodes. This resistance is derived as follows.

The standard current-voltage relation for a diode is

$$I(V_d) = I_0 \left[ \exp\left(\frac{eV_d}{mkT}\right) - 1 \right], \quad (5)$$

where  $e$  is the elementary charge,  $k$  is Boltzmann's constant,  $T$  is the absolute temperature, and  $V_d$  is the voltage across the diode.<sup>6</sup> At room temperature  $kT/e = V_{th} \approx 25 \text{ mV}$ . For a silicon diode factor  $m \approx 2$  and the reverse saturation current  $I_0$  is a few nanoamperes.<sup>6</sup> The application of Eq. (5) to antiparallel diodes as in Fig. 1 results in the current-voltage relation

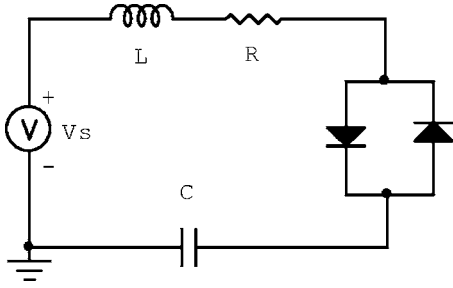


Fig. 1. The nonlinear circuit obtained from antiparallel diodes (1N4148), an inductor  $L=2.5 \mu\text{H}$ , and capacitor  $C=0.01 \mu\text{F}$ . The resistor  $R$  is included to account for the inherent resistance ( $9 \Omega$ ) of the inductor. The voltage source  $V_s$  is either a low frequency ( $\approx 1 \text{ Hz}$ ) square wave for the transient response experiments or sinusoidal for the steady-state driven oscillator experiments.

$$I(V_d) = 2I_0 \sinh\left(\frac{V_d}{mV_{th}}\right). \quad (6)$$

We define dimensionless quantities for the voltage and current,  $\nu = V_d/mV_{th}$  and  $i = I/2I_0$ . The current-voltage relation and dynamic resistance for the antiparallel diodes become  $i(\nu) = \sinh(\nu)$  or  $\nu(i) = \sinh^{-1}(i)$ , and

$$R_d(i) = \frac{dV_d}{dI} = \frac{mV_{th} d\nu}{2I_0 di} = \frac{mV_{th}}{2I_0 \cosh(\nu(i))} \\ = \frac{R_{max}}{\cosh(\sinh^{-1}(i))}. \quad (7)$$

Using values  $m=2$ ,  $V_{th}=25 \text{ mV}$ , and  $I_0=3 \text{ nA}$ , we find  $R_{max} = mV_{th}/(2I_0) = 8.3 = M\Omega$ .

Figure 2 shows the dynamic resistance, Eq. (7), as a function of the dimensionless current. The behavior of Eq. (7) for large and small currents is the same as Eq. (2) where  $b = R_{max}$ . The inverse current relation in Eq. (2) is generally known for a conducting diode ( $|i| \gg 1$ ) and is usually expressed as  $(25/I)\Omega$  (where  $I$  is in mA and  $m=1$  for an ideal diode).<sup>7</sup>

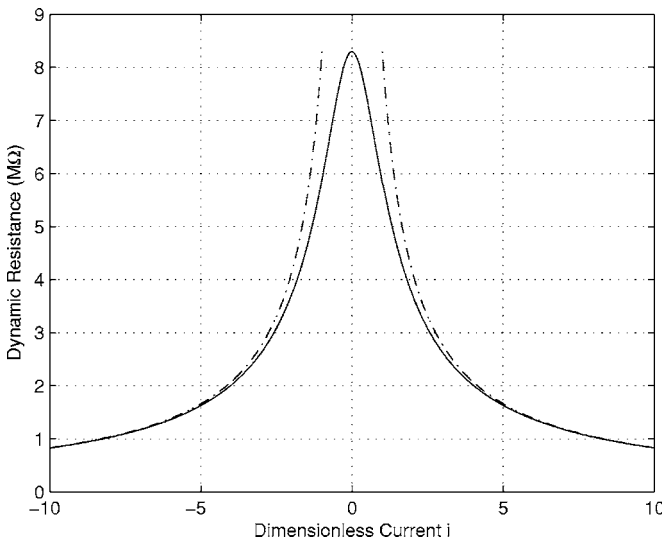


Fig. 2. The calculated dynamic resistance  $R_d(i)$  (solid line) for antiparallel diodes using Eq. (7). Also shown is the inverse current approximation  $R_{max}/|i|$  (dashed line). The dimensionless current is  $i = I/(2I_0)$ , where  $I$  is the current in amperes and  $I_0=3 \text{ nA}$  is the diode's reverse saturation current.

We define the dimensionless time  $\tau = t/\sqrt{LC}$  and use Eq. (4) to rewrite Eq. (3) for the transient response in terms of the dimensionless quantities:

$$\frac{d^2i}{d\tau^2} + \left( R\sqrt{\frac{C}{L}} + R_d(i)\sqrt{\frac{C}{L}} \right) \frac{di}{d\tau} + i = 0. \quad (8)$$

Thus we have shown that the circuit in Fig. 1 is described by Eqs. (1) and (2) where

$$b_0 = R\sqrt{\frac{C}{L}}, \quad (9a)$$

$$b_1(i) = R_d(i)\sqrt{\frac{C}{L}}, \quad (9b)$$

$$b = R_{max}\sqrt{\frac{C}{L}}. \quad (9c)$$

### III. METHODS

We apply Kirchhoff's voltage law to Fig. 1 and solve Eq. (6) for the voltage across the diodes to yield

$$\frac{dI}{dt} = \frac{-RI}{L} - \frac{mV_{th}}{L} \sinh^{-1}\left(\frac{I}{2I_0}\right) - \frac{V_C}{L} + \frac{V_s(t)}{L}, \quad (10a)$$

$$\frac{dV_C}{dt} = \frac{I}{C}. \quad (10b)$$

Equation (10) is solved numerically using an adaptive Runge-Kutta method in Matlab. The diodes are characterized by  $m=2$  and  $I_0=3 \times 10^{-9} \text{ A}$ , values obtained by measuring the diode's current-voltage characteristics and fitting to Eq. (5). This model was used to make predictions for all the experiments. However, Eq. (5) deviates from the measured I-V curve when used for both small and large currents.<sup>6</sup> For experiments involving large currents we used a second set of parameters,  $m=2.764$  and  $I_0=1.7 \times 10^{-7} \text{ A}$ , found by fitting current-voltage data for currents greater than 5 mA.

The initial conditions and  $V_s(t)$  for the transient response were chosen to match conditions used in the measurements—a square wave voltage source with frequency set low enough ( $\approx 1 \text{ Hz}$ ) so that each transition of the square wave gives a well-defined initial voltage  $V_0$  and final voltage  $V_f$  for the capacitor voltage. For the numerical solution,  $V_s(t)$  is  $V_f$ , and the initial conditions are zero current and  $V_0$  for the capacitor voltage.

For the steady-state response  $V_s(t)$  is a sinusoidal function. Solutions are computed for different source amplitudes and frequencies. The amplitude of the computed capacitor voltage is recorded after the transient response is gone so that the solution has clearly achieved steady-state. The voltage gain  $A$  of the circuit is the ratio of voltage amplitudes of the capacitor and the source. The results of the numerical solutions for the steady-state are predictions for the gain, the resonant frequency, and the sharpness of the resonance as functions of the source amplitude.

Data were collected on a Tektronix TDS 1002 digital oscilloscope. A standard  $10 \text{ M}\Omega$  oscilloscope probe attached to the capacitor will affect the circuit's behavior because  $10 \text{ M}\Omega$  is comparable to the dynamic resistance in Fig. 2 for

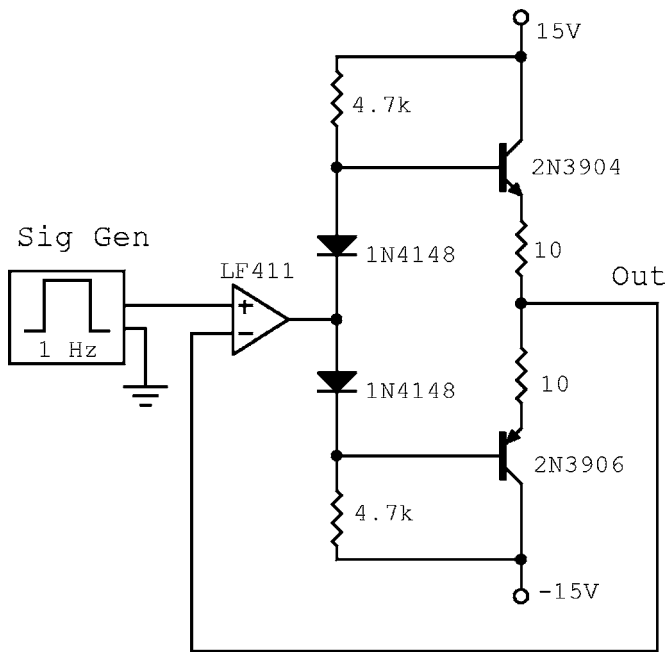


Fig. 3. Standard push-pull driver used with the signal generator in the antiparallel diodes-LC circuit. This use is necessary because the output impedance of most signal generators is too high to drive the circuit. General purpose op amps and transistors suffice. We used LF411, 2N3904, and 2N3906. A simpler driver omits the diodes and the 4.7 k $\Omega$  and 10  $\Omega$  resistors and connects the op amp output directly to the bases of the transistors. This simplification adds a small cross-over glitch to the signal from the signal generator.

small currents. Therefore the capacitor voltage was buffered by a unity gain FET input op amp (LF411 for example) before measurements by the oscilloscope.<sup>8</sup>

The quality of the low frequency square wave source  $V_s$  used in the transient response is important. The transition should be complete in a time much shorter than the natural oscillation period,  $2\pi\sqrt{LC} \approx 30 \mu\text{s}$  for  $L=2.5 \text{ mH}$  and  $C=0.01 \mu\text{F}$ . A square wave from a typical signal generator will not be able to drive the circuit due to the relatively high output impedance of the signal generator. Therefore we used the drive circuit shown in Fig. 3. The result is a square wave with transitions completed within 1  $\mu\text{s}$ .

For the steady-state measurements a sinusoidal voltage with the desired amplitude and frequency is provided by the signal generator and drive circuit. To investigate how the maximum gain  $A_{\text{max}}$  depends on the source amplitude, the frequency was adjusted to maximize the capacitor voltage for each source amplitude. This procedure also provided data for how the resonant frequency depends on source amplitude. To investigate the sharpness of the resonance response, the capacitor voltage was measured as a function of frequency at two source amplitudes.

It is important to consider the capacitor's equivalent series resistance. Using a general purpose ceramic disk capacitor without including its equivalent series resistance will result in poor agreement between measurement and prediction. We minimize the equivalent series resistance by using five nominal 0.002  $\mu\text{F}$  polypropylene capacitors in parallel. The equivalent series resistance of this combination appeared to be no more than 1  $\Omega$ .

Using a 0.01  $\mu\text{F}$  ceramic disk capacitor instead of the polypropylene capacitors required adding 15  $\Omega$  to the induc-

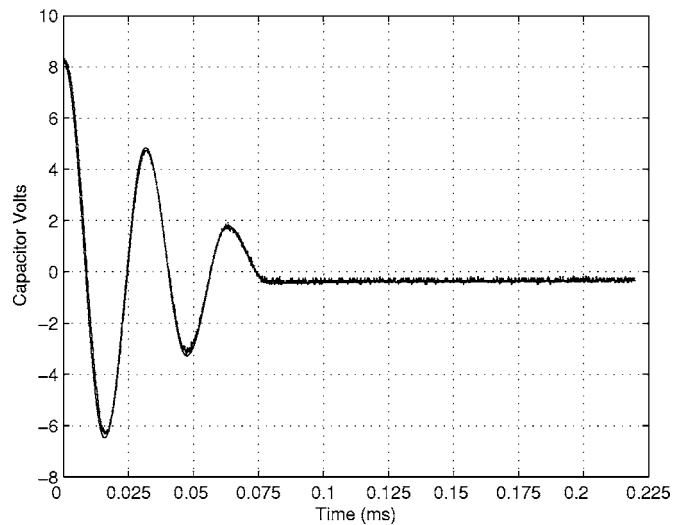


Fig. 4. Transient response of the capacitor voltage when the square wave source  $V_s$  makes a transition from 8.2 to 0 V at  $t=0$ . The numerical result (smooth line) and measured response (noisy line) are nearly indistinguishable. Note that a transition from underdamped to overdamped behavior occurs near  $t=0.075 \text{ ms}$ . As described in the text the overdamped decay to zero is comparatively slow and is not complete in the plot.

tor's 9  $\Omega$  to obtain good agreement between measurement and numerical prediction. Thus the equivalent series resistance  $R_{\text{esr}}$  of the ceramic capacitor is about 15  $\Omega$ . The predicted value of  $R_{\text{esr}}$  is obtained by using the dissipation factor from the capacitor data sheet stated as less than 0.03, and the relation for the dissipation factor  $\omega R_{\text{esr}} C$ .<sup>9</sup> At the natural oscillation frequency of approximately 30 kHz, the predicted value of  $R_{\text{esr}}$  for the 0.01  $\mu\text{F}$  ceramic capacitor is 16  $\Omega$ . This value compares well with our results.

#### IV. RESULTS AND DISCUSSION

Figure 4 shows the data and the numerical solution for the transient response of the voltage across the capacitor. The oscillator makes a transition from underdamped to overdamped behavior when the amplitude (peak capacitor voltage) decreases below a threshold value. The last zero crossing occurs at 0.075 ms. After this time the voltage reaches a maximum, then undergoes monotonic decay characteristic of an overdamped oscillator. The decay is not obvious in Fig. 4 because it is very slow due to the diode's large dynamic resistance for small currents. The decay of the voltage drop across the capacitor was nearly logarithmic, requiring about 0.5 s for the 0.01  $\mu\text{F}$  capacitor to be essentially discharged.<sup>8</sup> The use of the low frequency ( $\approx 1 \text{ Hz}$ ) square wave source allows this decay to be completed before the next transition of the square wave.

The transition from underdamped to overdamped behavior may be understood by considering the transient response oscillation frequency for a standard RLC circuit:

$$f = \frac{\omega}{2\pi} = \frac{1}{2\pi} \sqrt{\frac{1}{LC} - \left(\frac{R}{2L}\right)^2}. \quad (11)$$

For a fixed value of  $R$  the frequency is constant so there is no transition from underdamped to overdamped behavior for the standard RLC circuit. For the antiparallel diodes the resistance depends on the current as shown in Fig. 2. If  $R$  repre-

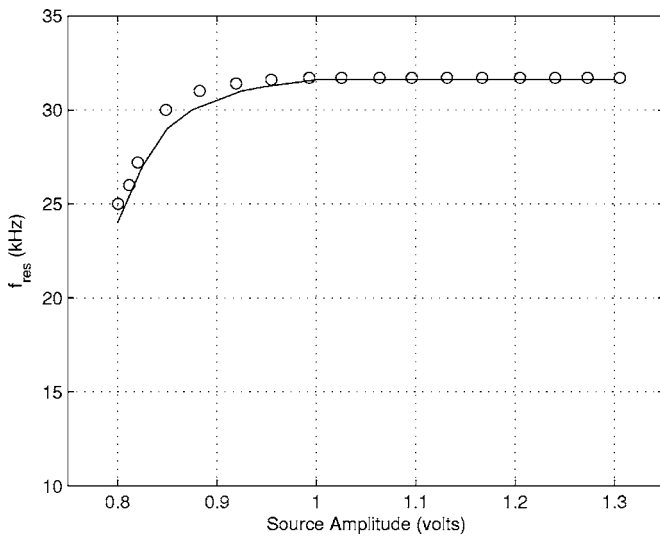


Fig. 5. The resonant frequency as a function of the source amplitude. The resonance was identified by adjusting the frequency to maximize the capacitor voltage amplitude for each source amplitude. The numerical results are lines and measured data are circles.

sents an effective resistance during a complete oscillation, then Eq. (11) predicts the dependence of the frequency on the amplitude. As the amplitude decreases, the current becomes smaller, causing the dynamic resistance of the antiparallel diodes and the effective resistance to increase. Eventually the effective resistance is sufficiently large so that the right-hand side of Eq. (11) becomes imaginary, corresponding to the transition to overdamped decay. The concept of an effective resistance is useful for understanding the observed behavior, but it is not intended as a calculation tool.

The characteristics of interest for the steady-state driven oscillator are the voltage gain  $A$ , the resonant frequency, and the sharpness of the resonance. These characteristics are independent of the source amplitude for the standard RLC circuit. We will use the standard RLC results to understand the amplitude-dependent behavior of the antiparallel diodes-LC circuit.

Figures 5 and 6 show how the resonance frequency  $f_{\text{res}}$  and the maximum gain  $A_{\text{max}}$  depend on the source amplitude. To understand these results consider the theoretical voltage gain  $A$  for the standard RLC circuit:

$$A = \frac{1}{LC\sqrt{(\omega R/L)^2 + (\omega^2 - 1/LC)^2}}. \quad (12)$$

The maximum gain occurs at the resonance frequency,

$$f_{\text{res}} = \frac{\omega_{\text{res}}}{2\pi} = \frac{1}{2\pi} \sqrt{\frac{1}{LC} - \frac{1}{2} \left(\frac{R}{L}\right)^2}. \quad (13)$$

[Note that Eq. (13) differs from Eq. (11), the natural oscillation frequency for the transient response of the standard RLC circuit. The similarity of these relations is an easy source of confusion.] The evaluation of Eq. (12) at resonance gives the maximum gain

$$A_{\text{max}} = \frac{1}{RC\sqrt{1/LC + (R/2L)^2}}. \quad (14)$$

Clearly  $A_{\text{max}}$  and  $f_{\text{res}}$  do not depend on the source amplitude for the standard RLC circuit. However, if we take  $R$  to rep-

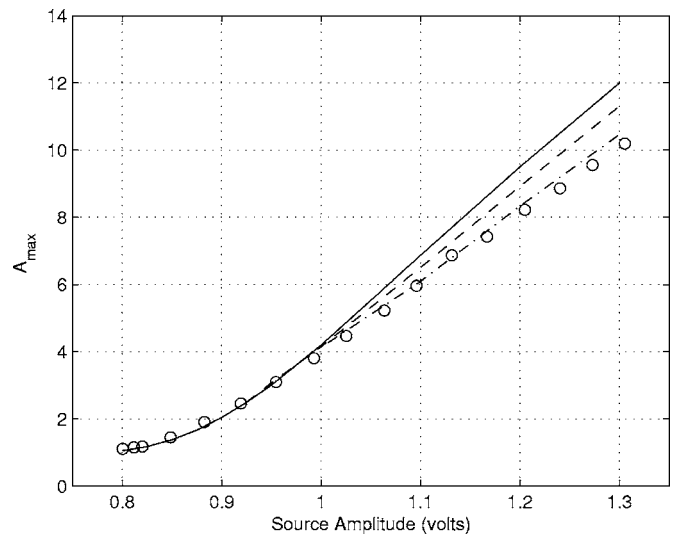


Fig. 6. The maximum voltage gain  $A_{\text{max}}$  as a function of the source amplitude.  $A_{\text{max}}$  is the ratio of the voltage amplitudes of capacitor and source at the resonant frequency. The solid line is the result using the single parameter set for the diode  $I$ - $V$  characteristics and the dashed line is the prediction when an additional set of diode parameters was included for high currents as described in Sec. III The dot-dashed line includes  $1 \Omega$  for the capacitor's equivalent series resistance.

resent the effective resistance of the antiparallel diodes, then Figs. 5 and 6 should be similar to graphs of Eqs. (13) and (14). In Fig. 7 we choose  $1/R$  for the abscissa because increasing the source amplitude correlates with decreasing the effective resistance of the diodes.

Figure 7 shows the critical value  $1/R_{\text{crit}}$  analogous to the source amplitude  $0.8 \text{ V}$  in Figs. 5 and 6 at which  $f_{\text{res}}$  drops sharply and  $A_{\text{max}}=1$ .  $R_{\text{crit}}$  is found by setting  $f_{\text{res}}=0$  in Eq. (13), giving

$$R_{\text{crit}} = \sqrt{\frac{2L}{C}}. \quad (15)$$

At  $R=R_{\text{crit}}$  a standard RLC circuit makes a smooth transition from a resonant oscillator with  $f_{\text{res}}$  given by Eq. (13) to a

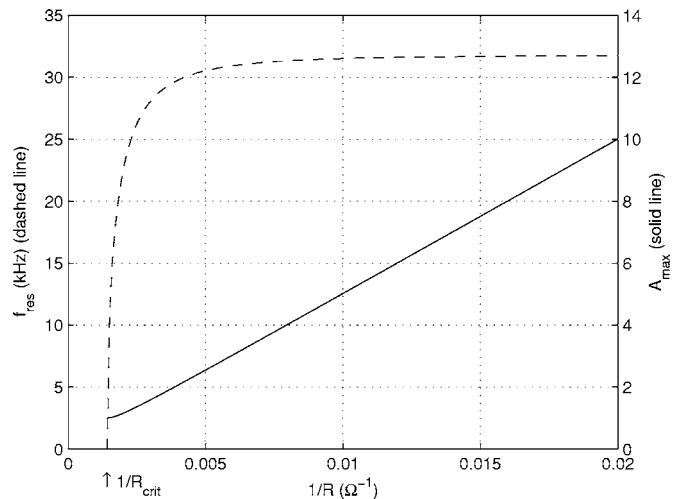


Fig. 7. Calculated resonant frequency (dashed line), Eq. (13), and maximum gain (solid line), Eq. (14), for the standard RLC circuit versus  $1/R$  ( $L=2.5 \text{ mH}$  and  $C=0.01 \mu\text{F}$ ). The resonant frequency drops to zero and  $A_{\text{max}}=1$  at  $R_{\text{crit}}=707 \Omega$  ( $1/R_{\text{crit}}=0.0014 \Omega^{-1}$ ).

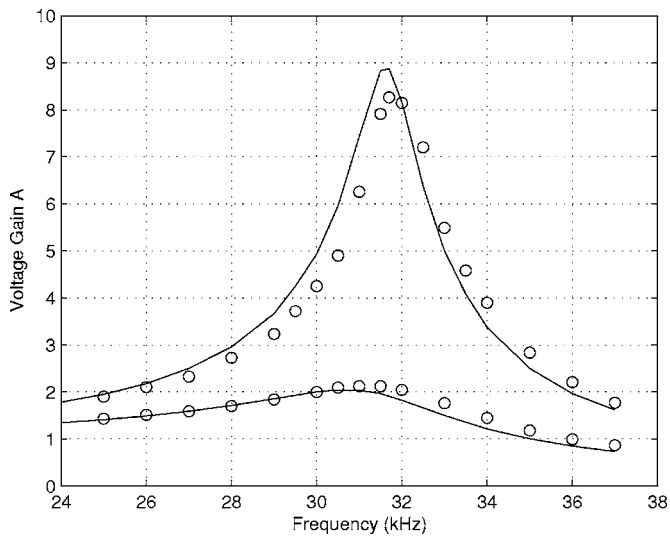


Fig. 8. The frequency response of the voltage gain  $A$  for two source amplitudes: 0.9 V (lower) and 1.2 (upper) V. The 1.2 V numerical results used the two-part parametrization for the diodes corresponding to the dashed line result in Fig. 5.

cutoff filter with  $f_{\text{res}}=0$ . An estimate of the diodes' effective resistance at the transition (where  $A_{\text{max}}=1$ ) is made by setting  $L=2.5$  mH and  $C=0.01$   $\mu\text{F}$  in Eq. (15), giving  $R_{\text{crit}}=707$   $\Omega$  (at  $1/R_{\text{crit}}=0.0014$   $\Omega^{-1}$  in Fig. 7). At the source amplitude 1.3 V the gain in Fig. 6 is 10, corresponding to an effective resistance of 50  $\Omega$  (from  $1/R=0.02$   $\Omega^{-1}$  in Fig. 7).

Thus the conceptually simple picture emerges that the steady-state antiparallel diodes-LC circuit behaves like a RLC oscillator with a resistance that is determined by the source amplitude. It follows that the frequency response should sharpen as the source amplitude increases as is confirmed by the frequency response curves shown in Fig. 8.

The behavior for source amplitudes below 0.8 V is not like that of a RLC circuit with amplitude-dependent resistance. The resonant frequency does not drop to zero as occurs for the RLC circuit when  $R > R_{\text{crit}}$ . Instead the resonance response becomes nonsinusoidal and the gain drops below one. This small resonance peak is in addition to the unity

gain peak at  $f=0$  that occurs for the RLC circuit when  $R > R_{\text{crit}}$ . At small enough source amplitude the resonance peak at  $f \neq 0$  disappears (in our case at source amplitude 0.57 V there is a just barely detectable gain peak of 0.32 at 11.5 kHz), leaving only the  $f=0$  peak.

The ability to implement basic mathematical functions using common electrical components is useful for studying nonlinear systems.<sup>10,11</sup> In this paper the antiparallel diodes provide a dynamic resistance given by Eqs. (2) and (7), which results in interesting nonlinear behavior.

## ACKNOWLEDGMENTS

This research was supported by an award from the Research Corporation. M.L. was supported in part by the Undergraduate Research Assistantship Program at UNCG. We thank David Birnbaum for valuable suggestions.

<sup>a)</sup>Electronic mail: ehellen@uncg.edu

<sup>b)</sup>Current address: Columbia University, Department of Applied Physics and Applied Mathematics, New York, NY 10027.

<sup>1</sup>P. S. Linsay, "Period doubling and chaotic behavior in a driven anharmonic oscillator," *Phys. Rev. Lett.* **47**, 1349–1352 (1981).

<sup>2</sup>J. Testa, J. Perez, and C. Jeffries, "Evidence for universal chaotic behavior of a driven nonlinear oscillator," *Phys. Rev. Lett.* **48**, 714–717 (1982).

<sup>3</sup>R. W. Rollins and E. R. Hunt, "Exactly solvable model of a physical system exhibiting universal chaotic behavior," *Phys. Rev. Lett.* **49**, 1295–1298 (1982).

<sup>4</sup>R. Van Buskirk and C. Jeffries, "Observation of chaotic dynamics of coupled nonlinear oscillators," *Phys. Rev. A* **31**, 3332–3357 (1985).

<sup>5</sup>A. Iobe and Y. Abe, "Experimental observation of indeterminate transition in a driven R-L-diode resonator," *Physica D* **116**, 355–362 (1998).

<sup>6</sup>J. Millman and C. C. Halkias, *Electronic Devices and Circuits* (McGraw-Hill, New York, 1967), pp. 124–129.

<sup>7</sup>M. H. Jones, *A Practical Introduction to Electronic Circuits*, 3rd ed. (Cambridge U. P., Cambridge, 1995), p. 125.

<sup>8</sup>E. H. Hellen, "Verifying the diode-capacitor circuit voltage decay," *Am. J. Phys.* **71**, 797–800 (2003).

<sup>9</sup>I. J. Bahl, *Lumped Elements for RF and Microwave Circuits* (Artech House, Norwood, MA, 2003), p. 170.

<sup>10</sup>J. C. Sprott, "A new class of chaotic circuit," *Phys. Lett.* **266**, 19–23 (2000).

<sup>11</sup>J. C. Sprott, "Simple chaotic systems and circuits," *Am. J. Phys.* **68**, 758–763 (2000).